JOURNAL OF SOLID STATE CHEMISTRY 114, 326–336 (1995)

The Crystal Structure of Ba–β-Alumina Materials for High-Temperature Catalytic Combustion

Gianpiero Groppi,* Fabio Assandri,* Maurizio Bellotto,†,‡ Cinzia Cristiani,* and Pio Forzatti*,[1]

*Dipartimento di Chimica Industriale e Ingegneria Chimica, G. Natta del Politecnico, P.za Leonardo da Vinci 32, I-20133 Milano, Italy; and †CISE, P.O. Box 12081, 20134 Segrate, Milano, Italy

Received September 20, 1993; in revised form March 29, 1994; accepted April 4, 1994

Structure refinement through Rietveld analysis has been performed on a series of Ba–Al–O samples with Al/Ba ratios in the range 9–14. This material is considered for its potential use in catalytic combustion. The results show that different β-Al_2O_3-type structures are obtained upon calcination at 1670 K depending on the Al/Ba ratio. A β_{II}-Al_2O_3 phase forms for the lowest Al/Ba ratio and a β_I-Al_2O_3 forms for the highest one. Small amounts of additional phases are present in the samples with the border compositions. For an in-between composition (Al/Ba = 12) a monophasic sample is obtained with crystal structure and calculated cell parameters intermediate between those of β_I and β_{II}. The sample with the intermediate composition exhibits the highest surface area. A strict relationship between surface area and aspect ratio of the crystallites has been observed. This indicates that the sintering resistance of these materials derives from the suppression of crystal growth along the crystallographic axis c. Experimental data also indicate that sintering resistance is closely related to Ba content.

1. INTRODUCTION

Catalytic combustion is widely used for off-gas clean up and for low-power energy production. More recently it has also been considered as a promising method for the effective combustion of lean fuel–air mixtures in gas turbines with minimum emission of NO_x, CO, and unburnt hydrocarbons (1–3). Power application poses demanding requirements on the catalytic material in view of the extreme operating conditions typical of the combustor (T = 1470–1570 K, P = 10–15 atm, v_{gas} = 10–40 m/s). Hence the catalytic materials must present high thermal stability and high resistance to thermal shocks typical of gas turbine operation (1–4).

Among the investigated systems Ba–Al oxides appear to be promising materials due to their excellent thermal stability. Arai and co-workers (5–7) observed that the optimum thermal stability is attained for a Al/Ba ratio of 12 due to the formation of barium hexaaluminate ($BaO \cdot 6Al_2O_3$). They observed that the surface area of such a material depends on the preparation method as well as on stoichiometry. According to the phase diagram of BaO–Al_2O_3 (8) a single phase of composition $BaO \cdot 6Al_2O_3$ is stable up to its melting point of 2185 K in the composition range between Ba/Al = 0 and Ba/Al = 0.5 together with the neighboring α-Al_2O_3 and $BaO \cdot Al_2O_3$.

The high thermal resistance against sintering has been related to the peculiar layered structure of barium hexaaluminate. This structure consists of spinel blocks separated by planes where the large Ba cations are located (9). The layered structure suppresses crystal growth along the c axis (perpendicular to the Ba planes); this eventually accounts for the observed plate-like shape of the crystallites (6, 7).

The phase composition and the crystal structure of Ba–hexaaluminates have been widely investigated in the literature (10–13). It is worth noting that although $BaO \cdot 6Al_2O_3$ has been described to be monophasic, it is now well established that this compound is actually constituted by two distinct phases with defective β-Al_2O_3 structure. The ideal structure of β-Al_2O_3 is characterized by hexagonal symmetry. It is constituted by Al spinel blocks of composition $[Al_{11}O_{16}]^+$ intercalated by planes of composition [MO] containing monovalent or divalent cations and oxygen. One spinel block and one intercalating plane, that is also a mirror plane of the structure, constitute a semicell, the crystallographic cell containing two of both, as shown in Fig. 1. Wide deviations from stoichiometry for β-aluminas have been reported frequently in the literature (14). These deviations are usually caused by differences in the distribution of the cations in the mirror plane. Also for the Ba–β-aluminas the two observed phases differ in stoichiometry: β_I of composition $Ba_{1.5}Al_{22}O_{34.5}$ (Al/Ba = 14.67) is poorer in Ba, and β_{II} of composition $Ba_{2.33}Al_{21.33}O_{34.33}$ (Al/Ba = 9.15) is richer in Ba (12, 13). Structural details of these phases will follow.

Accordingly, a critical review of available literature data suggests that materials with the β-alumina structure,

‡ Present address: IFP, Rueil, France.

[1] To whom correspondence should be addressed.

0022-4596/95 $6.00

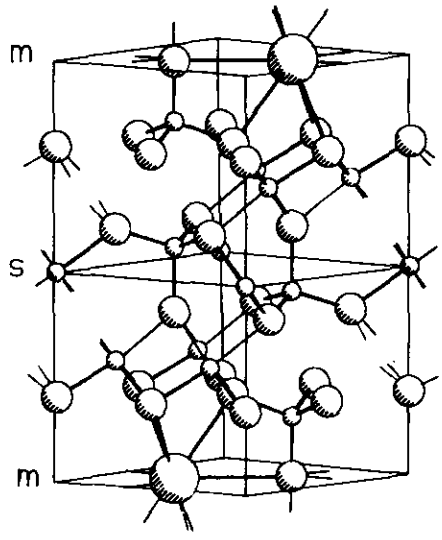

FIG. 1. Semicell of the ideal structure in β-Al_2O_3. Large spheres = alkaline or alkali earth metal; medium spheres = oxygen ions; small spheres = aluminum ions; m = mirror plane; s = spinel block.

which are of interest for catalytic purposes, can be obtained in a composition range between Al/Ba = 14.6 and Al/Ba = 9.1.

In previous papers (15, 16), the authors have reported on a new preparation method based on the precipitation of the constituents by $(NH_4)_2CO_3$ from an aqueous solution of the corresponding nitrates. This method provides a high interspersion of the constituents in the precursor and allows to obtain materials with good morphological properties.

In the present paper, the structural investigation on samples with Al to Ba atomic ratio from 14 to 9 is reported aiming to clarify the extent and nature of the defectivity in materials prepared using the above-cited method. The structure has been investigated by means of powder diffraction Rietveld refinement. The relations between the β_I and β_{II} phases and the relevance of compositional changes on the final morphological properties have also been addressed.

2. EXPERIMENTAL

Samples of $BaAl_xO_{(2+3x)/2}$ (x = 14, 12, and 9) were prepared using a coprecipitation method in aqueous medium (via carbonates) described elsewhere (15, 16), starting from the nitrates of the constituents, that typically provide a high interspersion of the constituents.

Chemical analysis, carried out by means of atomic adsorption (ICP-AES SPECTRO instrument by SPECTROFLAME), confirmed that quantitative precipitation occurred and that the actual Al/Ba ratios correspond to the nominal ones.

The precursors dried at 380 K and ground to 150–200 mesh were calcined at 1670 K according to the following calcination procedure: intermediate steps at 770, 970, 1070, 1270, 1370, 1470, 1570, and 1670 K, heating rate of 1 K/min, hold for 10 hr at each temperature step, and cooling rate 1.5 K/min. No grinding of the samples was performed after each heat treatment.

All the samples are quoted in the following with a notation indicating the ratio between the constituents; e.g., BaAl12 identifies the sample Ba–Al–O with Al/Ba = 12.

The crystal structure refinement was based on powder diffraction data. The powder patterns were collected in $\theta:2\theta$ step scanning mode, using Cu$K\alpha$ radiation and a diffracted beam monochromator (Philips vertical diffractometer PW1050-70). The step size used was 0.02° 2θ and the counting time was 10 sec/step. A divergent slit of 0.25° was used in order to keep the incident beam within the sample down to 5° 2θ. The patterns were measured in the range 15–130° 2θ. The refinement was performed with a Rietveld method (17). The general structure analysis system (GSAS) was used (18).

Surface area measurements were performed by the BET technique using N_2 adsorption (Fison Sorptomatic 1900 instrument).

3. STRUCTURAL MODELS

Two distinct Ba-β-Al_2O_3 phases, namely β_I and β_{II}, are detailed in the literature. The differences between them are associated with distinct defective cells, originated for electroneutrality reasons that are characterized by Ba vacancies in the mirror planes, and by the related structure defectivity (12, 13).

The structural models, actually refined in this work for β_I and β_{II}, have been derived from the literature. In the case of β_I the space group $P6_3/mmc$ is assumed according to what was proposed by Yamamoto and Iyi (11, 12) and consistent with the observed systematic extinctions. The same space group has been assumed also for the β_{II} phase, even if the correct space group should be $P\bar{6}m2$ (13). Powder diffraction can hardly discriminate between centrosymmetric and noncentrosymmetric space groups and the former choice results in a significantly lower number of independent atomic positions. Moreover, no reflections of appreciable intensity violating the $P6_3/mmc$ space group have been observed and refinements conducted with the correct space group did not result in a better agreement with the experimental data. In order to include the possibility of β_{II}-defective cells, an interstitial Ba site has been introduced in the spinel block (site symmetry $3m$; $x = \frac{1}{3}$, $y = \frac{2}{3}$, $z \approx \frac{2}{5}$). Only one of the two interstitial Ba positions present in a defective semicell and generated by centrosymmetry is actually occupied.

The Rietveld refinement used allowed for the Lo-

rentzian peak width to be dependent on the reflection indexes, thus modeling a crystallite shape anisotropy (19). The thermal parameters of Ba in the mirror plane have been refined anisotropically in order to simulate a splitting of the position out of the $6m2$ site which is also shown by difference Fourier maps. In all the refinements soft constraints have been introduced between the Al–O distances of interstitial aluminums, because the low occupancy factor of these atoms does not allow their precise location. Finally, the occupancies of Ba, Al, and O have been constrained with each other as follows (constraint equations are reported in the relevant Tables 1b, 2b, 3b):

(i) in the case of β_I, the presence of Ba vacancies implies an equal number of Reidinger defects;

(ii) in the case of β_{II}, for each Ba vacancy in the mirror plane two interstitial Ba in the spinel block are introduced along with one triple Reidinger defect.

It has also been reported in the literature that the distribution of ideal and defective cells in β_{II} structure is not random. There is a definite tendency to form an in-plane superstructure ($a\sqrt{3} \times a\sqrt{3}$), which is only bidimensional and does not extend to the c axis, as revealed by selected area electron diffraction (SAED) (11, 13). This disordered superstructure typically results in a diffuse halo in the range 27–31° 2θ of the powder XRD spectrum (13). The superstructure has not been considered in the Rietveld refinement because a crystallographic model is assumed, and the halo has been included in the empirical background modulation. A more convenient and physically sound approach to the investigation of the origin of the observed halo is based on a noncrystallographic approach to the simulation of the superstructure. A model has been devised based on random stacking of layers and resulting in a monodimensionally disordered structure. The DIFFaX program has been used which exploits the recursive nature of stacking sequences in a statistical ensemble of crystallites (20). This algorithm generalizes the Hendriks and Teller (21) approach and is easily applicable to all crystal structures.

4. RESULTS

4.1. Structure

The powder patterns of the samples BaAl9, BaAl12, and BaAl14 calcined at 1670 K are reported in Fig. 2. It is shown that in BaA19 and BaAl14, phases other than β-aluminas are present, $BaAl_2O_4$ and α-Al_2O_3, respectively. Quantitative Rietveld analyses yielded 2% $BaAl_2O_4$ and 2% α-Al_2O_3 by weight. The usual accuracy of such an analysis is of the order of 1–2% (17). The sample BaAl12 appears to be monophasic. The inspection of the relative intensities of the β-alumina phases, particularly in the ranges 30–37° 2θ and 15–21° 2θ, suggests the presence of differences between their structures depending on the Ba content. Furthermore a diffuse halo is present in the range 27–31° 2θ in sample BaAl9 and, to a minor extent, in sample BaAl12. According to what proposed by Yamamoto and Iyi (11, 13) and discussed below, this feature can be attributed to the formation of a superstructure in the β_{II} phase. Thus, a β_{II}-type structure for sample BaAl9 and a β_I-type structure for sample BaAl14 have been hypothesized. For sample BaAl12 an intermediate structure has been assumed, which will be described in detail later on.

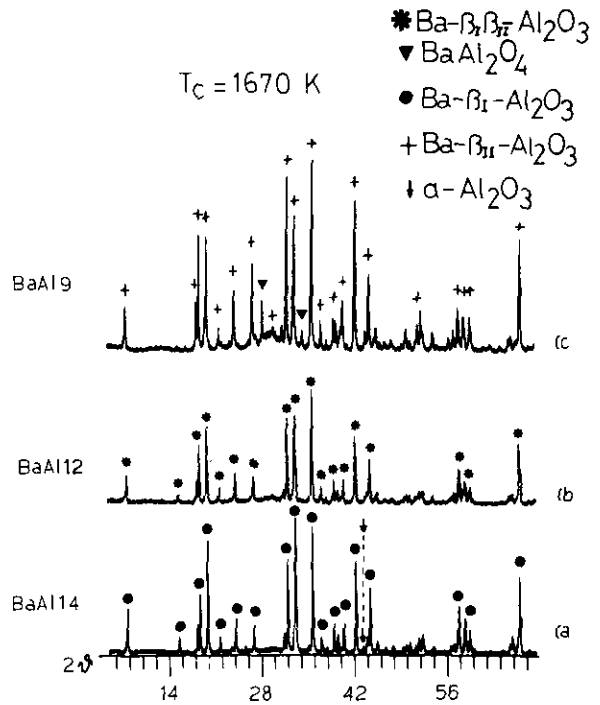

FIG. 2. X-Ray powder diffraction patterns of Ba–Al–O samples calcined at 1670 K: (a) BaAl14, (b) BaAl12, and (c) BaAl9.

BaAl14. The results of Rietveld refinement of sample BaAl14 are reported in Table 1a. The low value of χ^2 is an index of the correctness of the assumed model involving the presence of β_I and of small quantities of α-Al_2O_3. The calculated cell parameters of β_I ($a_0 = b_0 =$ 5.5876(2) Å, $c_0 = 22.7270(9)$ Å) compare well with those reported in the literature ($a_0 = b_0 = 5.587(2)$ Å, and $c_0 =$ 22.727(1) Å (12)). The phase composition reasonably accounts for the overall sample chemical composition ($(Al/Ba)_{calc} = 15.3$, $(Al/Ba)_{nom} = 14$). The calculated fraction of defective cells results in 0.283(4) compared to the theoretical value of 0.25 required by electroneutrality. The calculated atomic positions and thermal parameters for β_I-Al_2O_3 are reported in Table 1b. The high value of the anisotropic thermal factor U_{11}, compared to U_{33}, calculated for the barium atom, points to the fact that this atom is probably split out of the $6m2$ site and is consistent with

TABLE 1A
Results of Rietveld Structural Refinement of Sample BaAl14 Calcined at 1670 K

$\chi^2 = 0.80$	$R_{wp} = 16.9\%$
Phase composition	98% Ba-β_I-Al_2O_3 + 2% α-Al_2O_3
Nominal Al/Ba ratio	14
Calculated Al/Ba ratio	15.3
	Ba-β_I-Al_2O_3 phase
Space group	$P6_3/mmc$
Cell parameters	$a = b = 5.5876(2)$ Å
	$c = 22.727(1)$ Å
Theoretical β_I composition	$Ba_{0.75}Al_{11}O_{17.25}$
Calculated composition	$Ba_{0.72}Al_{11}O_{17.28}$
Crystallite shape factor	$(D/h) = 1.8$
	α-Al_2O_3 phase
Space group	$R - 3c$
Cell parameter	$a = b = 4.7650(9)$ Å
	$c = 13.030(4)$ Å

the known high mobility of the cations in the mirror plane of β-Al_2O_3 structures (14). The high value of the isotropic temperature factor for O(5), which is also probably split out of the position of symmetry (12), should also be noted. The interatomic distances and the bond angles are reported in Table 1c. They agree within 4 e.s.d. with literature data obtained by single-crystal refinement (12).

BaAl9. The results of Rietveld refinement of sample BaAl9 are reported in Table 2a. The higher value of χ^2 is probably due to difficulties in fitting the halo at 27–31° 2θ with an empirical background function (in this case a cosine Fourier series). The model involves the presence of β_{II} and barium aluminate phases. The calculated cell parameters of β_{II} ($a_0 = b_0 = 5.6016(3)$ Å, $c_0 = 22.906(1)$ Å) compare with those reported in the literature ($a_0 = b_0 = 5.6003(5)$ Å, and $c_0 = 22.922(2)$ Å) (13). Also in this case the phase composition accounts for the overall chemical composition of the sample ($(Al/Ba)_{calc} = 9.0$; $(Al/Ba)_{nom} = 9$). The calculated fraction of defective cells resulted in 0.314(6) compared to the theoretical value of 0.333 required by electroneurality. The calculated atomic positions and thermal parameters for the β_{II}-Al_2O_3 phase are reported in Table 2b. Also in this case the value of U_{11} is higher than the value of U_{33} for the barium atom in the mirror plane and O(5) has an abnormally high value of isotropic temperature factor. In the case of O(6) the high value calculated for the isotropic temperature factor is meaningless because of its poor accurancy due to the low occupancy. The interatomic distances and the bond angles are reported in Table 2c. In this case a direct comparison with literature data obtained by single-crystal refinement is not possible due to the different space groups adopted; however, the calculated values appear to be reasonable. It is worth noting that the Ba–O distances calculated for the 12-coordinate polyhedron are lower than those of the 9-coordinate polyhedron. This could result in a higher energy of the Ba site in the spinel block and is in line with the experimental evidence that β_{II} phase only forms in the presence of an excess of barium. Moreover, it must be noted that, compared to BaAl14, a small contraction of the regular Ba site is observed in this sample. This contraction brings about a distortion of the site, as it should, to maintain the Ba valency (22).

TABLE 1B
Results of Rietveld Structural Refinement on Ba-β_I-Al_2O_3 Phase in Sample BaAl14 Calcined at 1670 K

Atom	Site symm.	Mult.	Occupancy	X	Y	Z	U_{iso} ×100	U_{11} ×100	U_{33} ×100
Ba(1)	$6m2$	2	0.717(4)	0.3333	0.6667	0.750		3.4(1)	0.1(1)
Al(1)	m	12	0.906(1)	0.1673(3)	0.3345(6)	−0.1044(1)	1.64(8)		
Al(2)	$3m$	4	1.00	0.3333	0.6667	0.0239(2)	2.9(2)		
Al(3)	$3m$	4	1.00	0.3333	0.6667	0.1753(2)	2.3(2)		
Al(4)	$3m$	2	1.00	0.00	0.00	0.00	2.4(2)		
Al(5)[a]	m	12	0.094(1)	0.841(2)	0.682(3)	0.1745(7)	4(9)		
O(1)	m	12	1.00	0.1595(4)	0.3189(8)	0.500(2)	1.2(2)		
O(2)	m	12	1.00	0.5036(4)	1.0072(9)	0.1457(2)	1.9(2)		
O(3)	$3m$	4	1.00	0.333	0.6667	−0.0545(4)	1.8(3)		
O(4)	$3m$	4	1.00	0.00	0.00	0.1426(5)	0.9(3)		
O(5)	$6m2$	2	1.00	0.3333	0.6667	0.25	8.6(7)		
O(6)[a]	$mm2$	6	0.094(1)	0.875(5)	0.75(1)	0.25	0(2)		

Note. Constraints on occupancy: Ba(1) + 3 Al(5) = 1 (Reidinger defect); Al(1) + Al(5) = 1 (balance on Frenkel defect); Al(5) = O(6) (balance on oxygen bridge). Fraction of defective cells = 1 − Ba(1).

[a] Atoms in interstitial positions.

TABLE 1C
Calculated Interatomic Distances and Bond Angles for Ba–β_I-Al_2O_3 Phase in Sample BaAl14 Calcined at 1670 K

Interatomic Distances			Bond Angles	
Atoms	Number of bond	Distances (Å)	Atoms	Bond angles (°)
	Octahedral coordination		Octahedral coordination	
Al(1)–O(1)	2	2.009(4)	O(1)–Al(1)–O(1)	83.4(3)
Al(1)–O(2)	2	1.849(3)	O(1)–Al(1)–O(2)	90.4(2)
Al(1)–O(3)	1	1.967(5)	O(2)–Al(1)–O(2)	95.3(3)
Al(1)–O(4)	1	1.837(6)	O(3)–Al(1)–O(1)	89.4(2)
Al(4)–O(1)	6	1.916(4)	O(3)–Al(1)–O(2)	86.1(2)
			O(4)–Al(1)–O(1)	85.4(3)
	Tetrahedral coordination		O(4)–Al(1)–O(2)	98.6(2)
Al(2)–O(1)	3	1.784(4)	O(1)–Al(4)–O(1)	88.4(2)
Al(2)–O(3)	1	1.782(9)	O(1)–Al(4)–O(4)	91.5(2)
Al(3)–O(2)	3	1.780(5)		
Al(3)–O(5)	1	1.697(5)	Tetrahedral coordination	
Al(5)–O(2)	2	1.761(9)	O(1)–Al(2)–O(1)	109.5(2)
Al(5)–O(4)	1	1.70(2)	O(3)–Al(2)–O(1)	109.4(2)
Al(5)–O(6)	1	1.75(2)	O(2)–Al(3)–O(2)	106.6(3)
			O(2)–Al(3)–O(5)	112.2(2)
	9-Coordinated polyhedron		O(2)–Al(5)–O(2)	101.8(9)
Ba(1)–O(2)	6	2.847(5)	O(2)–Al(5)–O(6)	118(1)
Ba(1)–O(5)	3	3.2260(1)	O(4)–Al(5)–O(2)	107.6(7)
$(Ba–O)_{ave}$ = 2.973 Å			O(4)–Al(5)–O(6)	104(2)

In Fig. 3, the experimental pattern along with the simulated pattern derived by the DIFFaX calculation is reported. The model simulates the random stacking of an $(a\sqrt{3} \times a\sqrt{3})$ superstructure layer along the c axis. This superstructure involves the ordering of the defective cells in the ab plane. In the overall structure there is one such defective cell every two ideal cells. The stacking sequence involves an equal probability of finding the defective cell above any of the three cells constituting the superstructure unit layer. The physical meaning of this model is that the relative positions of defective cells are totally uncorrelated between neighboring conduction layers. The good agreement between the experimental and calculated pattern proves the correctness of the proposed model, confirming the presence of the disordered superstructure in the BaAl9 sample.

TABLE 2A
Results of Rietveld Structural Refinement of Sample BaAl9 Calcined at 1670 K

χ^2 = 1.83	R_{wp} = 14.95%
Phase composition	98% Ba–β_{II}-Al_2O_3 + 2% $BaAl_2O_4$
Nominal Al/Ba ratio	9
Calculated Al/Ba ratio	9.0
	Ba–β_{II}-Al_2O_3 phase
Space group	$P6_3/mmc$
Cell parameters	$a = b$ = 5.6017(3) Å
	c = 22.906(1) Å
Theoretical β_{II} composition	$Ba_{1.17}Al_{10.67}O_{17.17}$
Calculated composition	$Ba_{1.16}Al_{10.68}O_{17.16}$
Crystallite shape factor	(D/h) = 3.1
	$BaAl_2O_4$ phase
Space group	$P6_322$
Cell parameter	$a = b$ = 5.2345(5) Å
	c = 8.803(1) Å

BaAl12. The model adopted for the structure of BaAl12 is somewhat intermediate between β_I and β_{II}. It has been derived from the observations that the relative intensities for this sample are intermediate between those of samples BaAl14 and BaA19 and that a halo is present in the range 27–31° 2θ, even if less intense than for sample BaAl9. The structural model adopted here can be physically associated with an intergrowth between β_I and β_{II} phases. The intergrowth can occur according to indications in the literature (11, 22) due to the strong similarities between the two structures. The relevant constraints on site occupancies, due to the simultaneous presence of β_I and β_{II} defective cells, have been introduced (Table 3b).

The results of Rietveld refinement are reported in Table 3a. The low value of χ^2 supports the correctness of the adopted model. Also in this case the β-phase composition reasonably accounts for the overall chemical composition of the sample ($(Al/Ba)_{calc}$ = 12.7; $(Al/Ba)_{nom}$ = 12). The

TABLE 2B

Results of Rietveld Structural Refinement on Ba-β_{II}-Al_2O_3 Phase in Sample BaAl9 Calcined at 1670 K

Atom	Site symm.	Mult.	Occupancy	X	Y	Z	U_{iso} ×100	U_{11} ×100	U_{33} ×100
Ba(1)	$6m2$	2	0.843(3)	0.3333	0.6667	0.750		2.81(1)	1.9(2)
Ba(2)[a]	$3m$	4	0.157(3)	0.6667	0.3333	0.4697(5)	1.8(3)		
Al(1)	m	12	0.843(3)	0.1636(4)	0.3273(8)	−0.1034(2)	1.8(1)		
Al(2)	$3m$	4	0.843(3)	0.3333	0.6667	0.0231(3)	0.8(2)		
Al(3)	$3m$	4	1.00	0.3333	0.6667	0.1768(3)	3.3(2)		
Al(4)	$3m$	2	1.00	0.00	0.00	0.00	2.2(3)		
Al(5)[a]	*m*	*12*	*0.157(3)*	*0.841(1)*	*0.681(2)*	*0.1769(5)*	*1.4(6)*		
O(1)	m	12	1.00	0.1574(5)	0.315(1)	0.0485(3)	0.2(2)		
O(2)	m	12	1.00	0.5050(4)	1.0100(9)	0.1499(3)	0.7(2)		
O(3)	$3m$	4	0.843(3)	0.3333	0.6667	−0.0555(7)	0.4(5)		
O(4)	$3m$	4	1.00	0.00	0.00	0.1464(6)	0.8(3)		
O(5)	$6m2$	2	1.00	0.3333	0.6667	0.25	11(1)		
O(6)[a]	$mm2$	6	0.157(3)	0.894(5)	0.790(1)	0.25	19(6)		

Note. Constraints on occupancy: Ba(1) + Al(5) = 1 (triple Reidinger defect); Ba(2) + Al(2) = 1 (displacement of regular atoms by Ba(2)); Ba(1) + Ba(2) = 1 (balance on Ba); Al(1) + Al(5) = 1 (balance on Frenkel defect); Al(5) = O(6) (balance on oxygen bridge); Al(2) = O(3) (displacement of regular atoms by Ba(2)). Fraction of defective cells 2 * [1 − Ba(1)] = 2 * Ba(2).

[a] Atoms in interstitial positions.

TABLE 2C

Calculated Interatomic Distances and Bond Angles for Ba-β_{II}-Al_2O_3 Phase in Sample BaAl9 Calcined at 1670 K

Interatomic Distances			Bond Angles	
Atoms	Number of bond	Distances (Å)	Atoms	Bond angles (°)
Octahedral coordination			Octahedral coordination	
Al(1)–O(1)	2	2.002(5)	O(1)–Al(1)–O(1)	82.7(4)
Al(1)–O(2)	2	1.930(5)	O(1)–Al(1)–O(2)	93.8(2)
Al(1)–O(3)	1	1.978(9)	O(2)–Al(1)–O(2)	89.5(3)
Al(1)–O(4)	1	1.863(8)	O(3)–Al(1)–O(1)	89.7(2)
Al(4)–O(1)	6	1.889(5)	O(3)–Al(1)–O(2)	86.2(4)
			O(4)–Al(1)–O(1)	*88.9(4)*
Tetrahedral coordination			O(4)–Al(1)–O(2)	95.1(3)
Al(2)–O(1)	3	1.804(6)	O(1)–Al(4)–O(1)	88.9(3)
Al(2)–O(3)	1	1.80(2)	O(1)–Al(4)–O(1)	91.1(3)
Al(3)–O(2)	3	1.776(5)		
Al(3)–O(5)	1	1.677(7)	Tetrahedral coordination	
Al(5)–O(2)	2	1.745(6)	O(1)–Al(2)–O(1)	110.1(3)
Al(5)–O(4)	1	1.696(9)	O(3)–Al(2)–O(1)	108.8(3)
Al(5)–O(6)	1	1.752(9)	O(2)–Al(3)–O(2)	108.6(3)
			O(2)–Al(3)–O(5)	110.3(3)
9-Coordinated polyhedron			O(2)–Al(5)–O(2)	102.2(8)
Ba(1)–O(2)	6	2.778(6)	O(2)–Al(5)–O(6)	119(1)
Ba(1)–O(5)	3	3.2341(2)	O(4)–Al(5)–O(2)	109.0(4)
$(Ba(1)–O)_{ave}$ = 2.973 Å			O(4)–Al(5)–O(6)	97(1)
Ba inside the spinel blocks (12-coordinated polyhedron)				
Ba(2)–O(1)	3	2.485(9)		
Ba(2)–O(1)	6	2.833(2)		
Ba(2)–O(2)	3	3.16(1)		
$(Ba(2)–O)_{ave}$ = 2.825 Å				

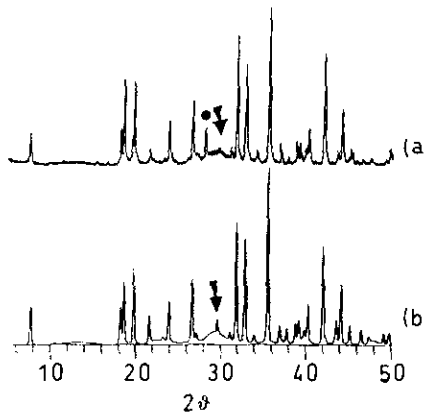

FIG. 3. Comparison between (a) experimental pattern of BaAl9 calcined at 1670 K and (b) calculated DIFFaX spectrum. ● = $BaAl_2O_4$; ♦ = diffuse halo.

fraction of β_I- and β_{II}-defective cells calculated on the basis of the site occupancies resulted in 0.186(8) and 0.086(8), respectively. The refined-cell parameters are intermediate between those reported in the literature for β_I and β_{II}. The atomic positions and thermal parameters for the β-alumina are reported in Table 3b and the interatomic distances and bond angles are reported in Table 3c. The calculated values are similar to those obtained for BaAl14 and BaAl9. Also in this case the value of U_{11} is higher than the value of U_{33} for the barium atom in the mirror plane and O(5) shows a high value of the isotropic temperature factor.

4.2. *Morphology*

It has been reported in the literature that Ba–β-Al_2O_3 consists of hexagonal plate-like crystals characterized by a strong anisotropy.

As stated above, Rietveld analysis allows us to describe the shape-anisotropy of the particles constituting our materials. The calculated value of the crystallites aspect ratio (i.e., the ratio between the average dimension parallel to the *ab* planes and the average dimension parallel to the *c* axis) for the β-Al_2O_3 of our Ba–Al–O samples are reported in Tables 1a, 2a, and 3a. For BaAl12 an aspect ratio of 7.4 has been obtained. This value is significantly higher than those obtained for BaAl9 and BaAl14 (3.1 and 1.8, respectively). The trend of surface-area values parallels that observed for the aspect ratios. In fact the highest value (15 m^2/g) is obtained for sample BaAl12 calcined at 1670 K, while surface areas significantly lower have been measured for BaAl14 and BaAl9. These data are consistent with literature indications (5–7) that report the highest thermal stability and the highest surface area for the BaAl12 systems.

5. DISCUSSION

Crystal structure refinement of Ba–Al–O samples has shown that different Ba–β-Al_2O_3-type structures are obtained upon calcination at 1670 K depending on the Al/Ba ratio. In line with indications in the literature (12, 13), β_{II} phase forms near the lowest Al/Ba (Al/Ba = 9) limit and β_I phase forms near the highest (Al/Ba = 14). Small amounts of additional phases (2% w/w α-Al_2O_3 and 2% w/w $BaAl_2O_4$) are present in the samples with the border compositions. These phases correspond to the neighboring ones reported in the phase diagram of the BaO–Al_2O_3 system. The correctness of the results of Rietveld analysis is supported by the good agreement between the calculated values of cell parameters, bond distances and angles, and the values reported in the literature for β_I (12) in the case of BaAl14 and for β_{II} (13) in the case of BaAl9. For an intermediate composition (Al/Ba = 12) a monophasic sample is obtained with crystal structure and cell parameters intermediate between those of β_I and β_{II}.

A halo is observed in the powder XRD spectrum of BaAl9 and, to a minor extent, of BaAl12. This feature has been successfully modeled assuming a random stacking sequence of *ab* planes showing an $a\sqrt{3} \times a\sqrt{3}$ superstructure. This confirms the presence of an in-plane superstructure disordered along the *c* axis associated with the β_{II} phase.

The structural details of the β-Al_2O_3 phases reported herein support and better clarify the formation mechanism reported in a previous paper (16). It has been observed that, under the preparation route here adopted, Ba–β-Al_2O_3 forms via solid-state reaction between microcrystalline γ-Al_2O_3 and dispersed Ba compounds or crystalline $BaAl_2O_4$ starting from a threshold temperature of 1370 K.

TABLE 3A
Results of Rietveld Structural Refinement of Sample BaAl12 Calcined at 1670 K

$\chi^2 = 1.46$	$R_{wp} = 18.77\%$
Phase composition	Ba–$\beta_I\beta_{II}$-Al_2O_3
Nominal Al/Ba ratio	12
Calculated Al/Ba ratio	12.7
Ba–$\beta_I\beta_{II}$-Al_2O_3 phase	
Space group	$P6_3/mmc$
Cell parameters	$a = b = 5.5936(4)$ Å
	$c = 22.767(2)$ Å
Nominal composition	$Ba_{0.90}Al_{10.89}O_{17.22}$
Calculated composition	$Ba_{0.86}Al_{10.91}O_{17.23}$
Crystallite shape factor	$(D/h) = 7.4$
Calculated ratio β_I/β_{II} cells	2.16

TABLE 3B
Results of Rietveld Structural Refinement on Ba–$\beta_I\beta_{II}$-Al_2O_3 Phase in Sample BaAl12 Calcined at 1670 K

Atom	Site symm.	Mult.	Occupancy	X	Y	Z	U_{iso} ×100	U_{11} ×100	U_{33} ×100
Ba(1)	6*m*2	2	0.771(7)	0.3333	0.6667	0.750		2.9(1)	1.4(3)
Ba(2)[a]	3*m*	4	0.043(4)	0.6667	0.3333	0.462(4)	8(4)		
Al(1)	*m*	12	0.894(7)	0.1662(4)	0.3325(8)	−0.1044(2)	1.5(1)		
Al(2)	3*m*	4	0.957(4)	0.3333	0.6667	0.0237(4)	2.7(2)		
Al(3)	3*m*	4	1.00	0.3333	0.6667	0.1758(3)	2.4(2)		
Al(4)	3*m*	2	1.00	0.00	0.00	0.00	1.5(3)		
Al(5)[a]	*m*	12	0.106(7)	0.839(1)	0.678(3)	0.1757(7)	1(1)		
O(1)	*m*	12	1.00	0.1579(6)	0.316(1)	0.0494(3)	1.3(2)		
O(2)	*m*	12	1.00	0.5027(6)	1.005(1)	0.1466(4)	1.9(2)		
O(3)	3*m*	4	0.957(4)	0.3333	0.6667	−0.053(1)	1.2(7)		
O(4)	3*m*	4	1.00	0.00	0.00	0.1451(7)	1.5(4)		
O(5)	6*m*2	2	1.00	0.3333	0.6667	0.25	9(1)		
O(6)[a]	*mm*2	6	0.106(7)	0.893(6)	0.78(1)	0.25	0(2)		

Note. Constraints on occupancy: Ba(1) − 2 Ba(2) + 3 Al(5) = 1 (Reidinger defect + triple Reidinger defect); Ba(2) + Al(2) = 1 (displacement of regular atoms by Ba(2)); Al(1) + Al(5) = 1 (balance on Frenkel defect); Al(5) = O(6) (balance on oxygen bridge); Al(2) = O(3) (displacement of regular atoms by Ba(2)); Fraction of defective β_I cells = 1 − Ba(1) − Ba(2); Fraction of defective β_{II} cells = 2 * Ba(2).

[a] Atoms in interstitial positions.

TABLE 3C
Calculated Interatomic Distances and Bond Angles for Ba–$\beta_I\beta_{II}$-Al_2O_3 Phase in Sample BaAl12 Calcined at 1670 K

Interatomic Distances			Bond Angles	
Atoms	Number of bond	Distances (Å)	Atoms	Bond angles (°)
Octahedral coordination			Octahedral coordination	
Al(1)–O(1)	2	2.011(6)	O(1)–Al(1)–O(1)	82.4(4)
Al(1)–O(2)	2	1.869(5)	O(1)–Al(1)–O(2)	91.2(3)
Al(1)–O(3)	1	2.00(2)	O(1)–Al(1)–O(3)	88.4(5)
Al(1)–O(4)	1	1.858(8)	O(1)–Al(1)–O(4)	86.9(4)
Al(4)–O(1)	6	1.898(5)	O(2)–Al(1)–O(2)	94.7(4)
			O(2)–Al(1)–O(3)	86.9(5)
Tetrahedral coordination			O(2)–Al(1)–O(4)	97.3(3)
Al(2)–O(1)	3	1.797(6)	O(1)–Al(4)–O(1)	88.5(3)
Al(2)–O(3)	1	1.74(3)	O(1)–A(4)–O(1)	91.5(3)
Al(3)–O(2)	3	1.770(6)		
Al(3)–O(5)	1	1.690(5)	Tetrahedral coordination	
Al(5)–O(2)	2	1.761(8)	O(1)–Al(2)–O(1)	110.0(3)
Al(5)–O(4)	1	1.70(1)	O(1)–Al(2)–O(3)	109.0(3)
Al(5)–O(6)	1	1.77(1)	O(2)–Al(3)–O(2)	106.8(4)
			O(2)–Al(3)–O(5)	112.0(4)
9-Coordinated polyhedron			O(2)–Al(5)–O(2)	102(1)
Ba(1)–O(2)	6	2.839(8)	O(2)–Al(5)–O(4)	107.6(6)
Ba(1)–O(5)	3	3.2295(2)	O(2)–Al(5)–O(6)	120(1)
$(Ba–O)_{ave}$ = 2.969 Å			O(4)–Al(5)–O(6)	97(2)
Ba inside the spinel blocks (12-coordinated polyhedron)				
Ba(2)–O(1)	6	2.81(1)		
Ba(2)–O(1)	3	2.61(7)		
Ba(2)–O(2)	3	2.95(9)		
$(Ba(2)–O)_{ave}$ = 2.792 Å				

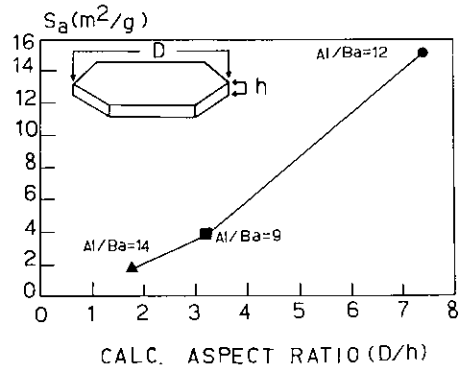

FIG. 4. Surface areas vs calculated aspect ratios of the β-Al_2O_3 crystallites in Ba–Al–O samples. ▲ Al/Ba = 14; ■ Al/Ba = 9; ● Al/Ba = 12.

The stabilization of γ-Al_2O_3 up to the formation temperature of the Ba–β-Al_2O_3 is due to the presence of dispersed barium which inhibits alumina sintering and phase transition. Considering structural analogy between the γ-Al_2O_3 and the β-Al_2O_3 structures, the formation of this last phase proceeds through the diffusion, along the oxygen close packed planes, of Ba ions in the spinel structure of γ-Al_2O_3 originating the discussed layered β-Al_2O_3 structure. The observed threshold temperature of 1370 K is related to the mobility of Ba in the Al_2O_3 matrix. The diffusion of Ba may be conceived to occur at the same rate along all oxygen planes at the beginning of the reaction, but the modification of the crystallographic field induced by Ba insertion prevents diffusion along adjacent planes resulting in the layered β-Al_2O_3 structure. According to this mechanism different structures (β_I or β_{II}) form depending on the local Ba activity. The intermediate structure observed in BaAl12, likely originated by an intergrowth of β_I and β_{II} domains, points to a uniform Ba activity throughout the sample.

In addition, the more difficult formation of Ba–β_{II}-Al_2O_3 in BaAl9, which occurs 100 K above that of β_I in BaAl14, can be due to the higher electrostatic energy associated with the 12-coordinated Ba site inside the spinel block, compared to the 9-coordinated Ba site in the mirror plane.

As stated above, the relevance of Ba–Al–O systems for catalytic applications is related to their thermal stability and particularly to their resistance against sintering. In line with the literature data, BaAl12 shows the maximum resistance against sintering. It retains a surface area of 15 m^2/g upon calcination at 1670 K for 10 hr. The same value was obtained by Arai and co-workers for a sample with identical composition prepared via hydrolysis of alkoxides and calcined at 1670 K. The high surface area retained by these samples is related to the plate-like shape developed by the crystallites. Arai and co-workers found an aspect ratio of 5–10 in their sample by means of TEM analysis (5–7) while our BaAl12 sample shows an aspect ratio of 7.4, as determined by XRD line profile analysis in Rietveld refinement.

The resistance to sintering in these materials has therefore been attributed to the anisotropic diffusion of atoms in the structure, caused by the layered β-Al_2O_3 structure suppressing diffusion parallel to the c axis (24, 25). The suppression of interlayer diffusion is suggested in the present work by the detection of the in-plane β_{II} superstructure. This superstructure arises from the lack of any interaction between successive Ba-containing planes which are stacked in a completely random fashion. However, the layered structure itself is not sufficient to provide a high resistance to sintering. Samples BaAl9 and BaAl14 exhibit surface areas significantly lower than BaAl12. Furthermore in our samples we have found different aspect ratios depending on the stoichiometry.

Figure 4, showing surface area vs aspect ratio, confirms the strict relationships between surface area and crystallite shape anisotropy, the higher surface area being exhibited by the most anisotropic sample.

In order to better clarify the different sintering behaviors of Ba–Al–O samples the surface area data vs calcination temperature in the range 1470–1670 K reported in Fig. 5 have to be considered. BaAl14 shows the maximum area at 1470 K (A_s = 32 m^2/g) but progressively sinters on increasing the calcination temperature up to the final value of 2 m^2/g. The surface area of BaAl12 slightly decreases from 1470 to 1570 K and keeps constant at 15 m^2/g upon further calcination at 1670 K. The surface area of BaAl9 calcined at 1470 K is significantly lower than those of BaAl14 and BaAl12 and further decreases to ≈6 m^2/g upon calcination at 1570 K. Anyway a surface area of ≈4 m^2/g is retained upon calcination at 1670 K. This behavior indicates that a critical Ba concentration in the structure is required for the effective suppression of crys-

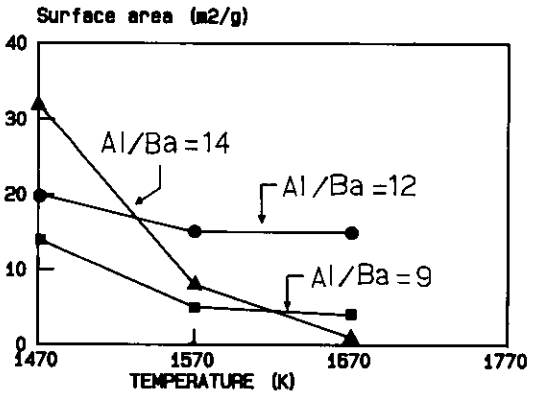

FIG. 5. Surface areas of Ba–Al–O samples vs calcination temperature.

tal growth along the c axis of Ba–β-Al_2O_3 crystallites. Indeed, in BaAl14, sintering proceeds even after the formation of Ba-β_I-Al_2O_3.

As stated above, β-Al_2O_3 structure does not allow the presence of adjacent Ba-containing planes, moreover the suppression of Ba diffusion between the layers prevents the reorganization of the stacking sequence of the layers along the c axis. Accordingly the reaction between two crystallites with Ba planes near the surface, resulting in a crystallite with close Ba containing planes, can hardly occur. The different behavior of Ba–Al–O samples points to the fact that in BaAl14, exhibiting a Ba–β_I-Al_2O_3 structure, a residual Ba mobility is retained possibly associated with the Ba vacancies in this structure. This mobility, allowing the reorganization of the stacking sequence, can be responsible for the sintering observed in BaAl14 on increasing the calcination temperature. On the other hand, the higher Ba content of BaAl9 and BaAl12, with total or partial character of β_{II} structure, prevents the growth along the c axis by limiting the possibility of the rearrangement of the stacking sequences.

The low surface area of BaAl9 is related to the slower formation rate of the β_{II} phase. The sintering of unreacted γ-Al_2O_3 and $BaAl_2O_4$ is likely responsible for the loss of surface area up to 1570 K. Once formed, the Ba-rich β_{II} phase does not sinter and retains the residual value of surface area.

6. CONCLUSIONS

The main conclusions of this work can be summarized as follows:

1. The coprecipitation method allowed us to obtain Ba–Al–O samples with a final layered β-Al_2O_3 structure in the Al/Ba range 9–14.

2. Rietveld structural refinements showed that different β-Al_2O_3 structures are obtained depending on Al/Ba ratio, namely β_{II}-Al_2O_3 for the highest Al/Ba ratio (Al/Ba = 9) and β_I-Al_2O_3 for the lowest ratio (Al/Ba = 14). For the in-between composition (Al/Ba = 12) a phase characterized by a structure intermediate between β_I and β_{II} has been observed. The good agreement between the calculated and the literature values of β_I and β_{II} of cell parameters, bond angles and distances, confirms the correctness of the structural models adopted. Only the sample with Al/Ba = 12 is monophasic. Small amounts of additional phases, namely α-Al_2O_3 (2%) in the case of Al/Ba = 14 and $BaAl_2O_4$ (2%) in the case of Al/Ba = 9, are present in the samples with the border compositions.

3. Due to the similarity between the structures of γ-Al_2O_3 and of β-Al_2O_3 a formation mechanism of the β phases is proposed which proceeds via diffusion of Ba ions in the oxygen close packed planes of γ-Al_2O_3. According to this mechanism the attainment of β_I or β_{II} structure only depends on the local Ba activity. In this scheme the intermediate Ba–$\beta_I\beta_{II}$-Al_2O_3 observed in the case of Al/Ba = 12 suggests the uniform Ba concentration in the crystallites.

4. In line with what is reported in the literature the superior morphological properties exhibited by the BaAl12 sample are related to the suppressed crystal growth along the c axis resulting in a strong shape anisotropy of the crystallites. The resistance to the sintering cannot be related only to the formation of a layered β-Al_2O_3-type structure. In fact it appears that a critical Ba content is required for the effective sintering inhibition as suggested by the worse morphological properties of BaAl14. For BaAl9 the lower surface area is likely related to the difficult formation of the final phase that results in an irreversible sintering of the precursor material.

ACKNOWLEDGMENTS

This study has been supported by the CNR-ENEL Project "Interaction of Energy Systems with Human Health and Environment"—Rome (Italy). The authors also thank Dr. Norberto Masciocchi for interesting suggestions and criticism.

REFERENCES

1. R. Prasad, L. A. Kennedy, and E. Ruckestein, *Catal. Rev. Sci Eng.* **26,** 1 (1984).
2. L. D. Pfefferle and W. C. Pfefferle. *Catal. Rev. Sci. Eng.* **29,** 219 (1987).
3. G. Groppi and P. Forzatti, *La Rivista dei Combustibili* **46,** 158 (1992).
4. R. M. Orenstein, M. B. Hilt, N. Abuaf, Y. Hara, Y. Furuse, and M. Fowlwe, Proceedings 91-Yokohama-IGTC-108, 1205 (1991).
5. M. Machida, K. Eguchi, and H. Arai, *J. Catal.* **103,** 385 (1987).
6. M. Machida, K. Eguchi, and H. Arai, *J. Am. Ceram. Soc.* **71,** 1142 (1988).
7. H. Arai, K. Eguchi, and M. Machida, MRS Int. Meeting on Advanced Materials, Vol. 2, p. 243, 1989.
8. E. M. Levin, C. R. Robbins, and H. F. McMurdie, *in* "Phase Diagrams for Ceramists" (M. K. Reser, Ed.), p. 97. The American Ceramic Society, 1985.
9. A. F. Wells, *in* "Structural Inorganic Chemistry," Oxford Univ. Press (Clarendon), London/New York, 1975.
10. S. Kimura, E. Bannai, and I. Shindo, *Mat. Res. Bull.* **17,** 209 (1982).
11. N. Yamamoto and M. O'Keeffe, *Acta Crystallogr., Sect. B* **40,** 21 (1984).
12. N. Iyi, Z. Inoue, S. Takekawa, and S. Kimura, *J. Solid State Chem.* **52,** 66 (1984).
13. N. Iyi, Z. Inoue, S. Takekawa, and S. Kimura, *J. Solid State Chem.* **60,** 41 (1985).
14. C. R. Peters, M. Bettman, J. W. Moore, and M. D. Glick, *Acta Crystallogr., Sect. B* **27,** 1826 (1971).
15. G. Groppi, M. Bellotto, C. Cristiani, P. Forzatti, and P. L. Villa, *Appl. Catal. A: General* **104,** 101 (1993).
16. G. Groppi, M. Belloto, C. Cristiani, and P. Forzatti, *J. Mater. Sci.* **29,** 3441 (1994).
17. J. E. Post and D. L. Bish, *in* "Modern Powder Diffraction," Vol. 20, p. 277. The Mineralogical Society of America, 1989.

18. A. C. Larson and R. B. Von Dreele, LANSCE, MS-H805, Los Alamos National Laboratory, Loa Alamos, NM 87545.
19. P. Thompson, D. E. Cox, and J. B. Hastings, *J. Appl. Crystallogr.* **20,** 79 (1987).
20. V. A. Drits and C. Tchoubar, *in* "X-ray Diffraction by Disordered Lamellar Structures," p. 33. Springer-Verlag, New York/Berlin, 1989.
21. S. Hendricks and E. Teller, *J. Chem. Phys.* **10,** 147 (1942).
22. M. O'Keefe and A. Navrotsky, *in* "Structure and Bonding in Crystals," Vol. II, Academic Press, New York 1981.
23. N. Iyi, Y. Bando, S. Takekawa, Y. Kitami, and S. Kimura, *J. Solid State Chem.* **64,** 220 (1986).
24. M. Machida, K. Eguchi, and H. Arai, *Bull. Chem. Soc. Jpn.* **61,** 3659 (1988).
25. M. Machida, T. Shiomitsu, K. Eguchi, H. Arai, and Y. Shimizu, *J. Solid State Chem.* **95,** 220 (1991).